Journal of Biomedical Optics

BiomedicalOptics.SPIEDigitalLibrary.org

Structural effects of simvastatin on rat liver tissue: Fourier transform infrared and Raman microspectroscopic studies

Sebnem Garip
Sevgi Haman Bayari
Mete Severcan
Sherif Abbas
Igor K. Lednev
Feride Severcan

SPIE.

Structural effects of simvastatin on rat liver tissue: Fourier transform infrared and Raman microspectroscopic studies

Sebnem Garip,[a,†] Sevgi Haman Bayari,[b,†] Mete Severcan,[c] Sherif Abbas,[d] Igor K. Lednev,[e] and Feride Severcan[e,*]

[a]Istanbul Kemerburgaz University, Department of Medical Biochemistry, Faculty of Medicine, Mahmutbey Dilmenler Caddesi, No: 26, Istanbul 34217, Turkey
[b]Hacettepe University, Department of Physics Engineering, Faculty of Engineering, Beytepe Campus, Ankara 06800, Turkey
[c]Middle East Technical University, Department of Electrical and Electronics Engineering, Faculty of Engineering, Dumlupinar Bulvari, No: 1, Ankara 06800, Turkey
[d]Middle East Technical University, Department of Biological Sciences, Faculty of Arts and Sciences, Dumlupinar Bulvari, No: 1, Ankara 06800, Turkey
[e]University at Albany, Department of Chemistry, State University of New York, Albany, New York 12222, United States

Abstract. Simvastatin is one of the most frequently prescribed statins because of its efficacy in the treatment of hypercholesterolemia, reducing cardiovascular risk and related mortality. Determination of its side effects on different tissues is mandatory to improve safe use of this drug. In the present study, the effects of simvastatin on molecular composition and structure of healthy rat livers were investigated by Fourier transform infrared and Raman imaging. Simvastatin-treated groups received 50 mg/kg/day simvastatin for 30 days. The ratio of the area and/or intensity of the bands assigned to lipids, proteins, and nucleic acids were calculated to get information about the drug-induced changes in tissues. Loss of unsaturation, accumulation of end products of lipid peroxidation, and alterations in lipid-to-protein ratio were observed in the treated group. Protein secondary structure studies revealed significant decrease in α-helix and increase in random coil, while native β-sheet decreases and aggregated β-sheet increases in treated group implying simvastatin-induced protein denaturation. Moreover, groups were successfully discriminated using principal component analysis. Consequently, high-dose simvastatin treatment induces hepatic lipid peroxidation and changes in molecular content and protein secondary structure, implying the risk of liver disorders in drug therapy. [DOI: 10.1117/1.JBO.21.2.025008]

Key words: simvastatin; liver; Fourier transform infrared imaging; Raman imaging; protein secondary structure; principal component analysis.

Paper 150764R received Nov. 11, 2015; accepted for publication Jan. 21, 2016; published online Feb. 18, 2016; corrected Apr. 8, 2016.

1 Introduction

Statins are cholesterol-lowering agents with proven efficacy and safety and are widely used for prevention of cardiovascular disease. Statins' action is through 3-hydroxy-3-methylglutaryl coenzyme A (HMG-CoA) reductase, which catalyzes the rate-limiting step of the cholesterol synthesis in liver and other tissues.[1–4] The increasing of the expression of hepatic low-density lipoprotein receptor (LDLR) is one of the most effective ways to lower plasma cholesterol levels.[5] Since cholesterol inhibits the expression of LDLR, by blocking cholesterol synthesis in the liver, statins activate hepatocyte LDLRs, increase the cellular cholesterol uptake and reduce the circulating low-density lipoprotein (LDL) cholesterol levels. This leads to improvements in cardiovascular risk by retarding atherosclerosis in all major arteries.

Among the statins, simvastatin, which is released to the market under the brand name Zocor, is one of the most frequently prescribed statins because of its efficacy in reducing LDL lipoprotein cholesterol levels, cardiovascular risk and related mortality, as well as its tolerability. It is used in doses of 5 to 80 mg. Our group previously reported that lower dose (20 mg/kg/day) has less side effects than high doses (50 mg/kg/day) in skeletal muscle.[6,7] Higher doses (160 mg) have been found to be too toxic, and perceived as overdose while giving only minimal benefit in terms of lipid lowering.[8]

The pleiotropic effects that are the beneficial effects beyond cholesterol lowering of statins have been previously investigated in clinical studies.[9–12] These effects include decreasing oxidative stress and inflammation,[9] neuroprotective effects on Alzheimer disease,[10] and improving bone strength.[13] There are also studies that report the adverse effects of statins on soft tissues such as muscle, peripheral nerves, liver, testis, and so on.[7,14–16] These effects of statins are mostly caused by the inhibition of mevalonate pathway. Statins also inhibit the nonsterol branch of the mevalonate pathway by inhibiting the HMC-CoA reductase.[17] Other adverse effects of mevalonate pathway inhibition by statins may be deficiency of coenzyme Q involved in mitochondrial electron transport and antioxidant protection, abnormal protein glycosylation due to dolichol shortage, or deficiency of selenoproteins.[18]

In literature, nuclear magnetic resonance (NMR) spectroscopy has been mostly used to investigate the simvastatin

*Address all correspondence to: Feride Severcan, E-mail: feride@metu.edu.tr

†These authors contributed equally to this study.

1083-3668/2016/$25.00

effects on serum lipid profiles of patients with hyperlipidemia or dyslipidemia.[19–23] LDL and high-density lipoprotein (HDL) particle number and particle size in serum samples of patients treated with ezetimibe/simvastatin[19] and niacin extended-release/simvastatin[21] combinations were measured with NMR spectroscopy to show the lipid-modifying benefits of simvastatin-drug combinations rather than other statin monotherapies in clinic studies. In the study of Insull et al.,[22] besides the particle number and size of LDL and HDL, percent changes in lipoproteins (apolipoprotein A1, apoB, and the apoB:A1) were also measured in the serum of simvastatin-treated-hyperlipidemic patients by NMR spectroscopy. All these studies showed the effective simvastatin treatment for lowering the serum lipids in the patients. In a recent study, NMR spectroscopy was also used for the investigation of lipid profiles in intact liver tissues.[24] In this study, endogenous metabolic profiles of intact liver tissues from simvastatin-treated hyperlipidemic hamsters were established using 1 H NMR spectroscopy. Liver triglyceride and cholesterol contents were reduced with lower levels of lactate, acetate, alanine, glutamine in liver samples of drug-treated hyperlipidemic hamsters than those in hyperlipidemic controls. Authors reported that simvastatin treatment might have a protective effect on liver under fatty liver condition.[24] In the study of Yang et al.,[25] high dose (80 mg/kg) simvastatin toxicity at the tissue level was studied by the analysis of toxicity markers (aspartate amino transferase, alanine amino transferase, and creatinine kinase) in urine samples of rats by an NMR-based study. The drug-induced cellular liver damage was also shown by histopathological liver data with H&E staining to support the NMR results.[25] Although NMR spectroscopy is an effective technique to establish the lipid profiles of body fluids and tissues, the most important disadvantage of this technique is the moderate sensitivity compared with other spectroscopic techniques. Compounds present in submillimolar and micromolar concentrations cannot practically be detected directly in tissues.[26] The presence of large lipid signals can also obscure much of the spectral region of interest such as proteins.[26]

In literature, immunohistochemistry, mRNA real time polymerase chain reaction (RT-PCR), and protein (multiplex assay, ELISA, western blot) analyses were also used to study the simvastatin effects on tissues.[27–29] Van der Meij et al. [29] investigated the simvastatin effects in reduction of vascular inflammation through lipid independent mechanism by using aortic wall samples of atherosclerotic patients treated with different doses (20 or 40 mg/day) of simvastatin. In the study, macrophage differentiation and activation was estimated by immunohistochemical staining, while expression of inflammation markers were measured by RT-PCR. Western blot analysis was used to determine the protein levels of cytokines/chemokines in aortic wall samples of simvastatin-treated patients. Authors reported that drug treatment selectively reduced macrophage-related inflammatory markers, while the other parameters did not show significant effect of simvastatin in reducing inflammation.[29] Ordinary biochemical and molecular biology techniques such as ELISA, western blot, and PCR are highly quantitative techniques in tissue studies, but they need long procedures of tissue homogenization and preexperimental preparation. Since they are experimentally challenging techniques, they also require significant effort for the optimization of conditions. Another disadvantage of these techniques is that molecular investigations can only be done in specific molecular groups such as proteins or DNA.

Information about the changes of molecular composition and physical/chemical environment of tissues has highly diagnostic value for disorders and diseases.[30] Vibrational spectroscopy has been used extensively for getting molecular structure information about tissues. As vibrational spectroscopic techniques, the potential of infrared and Raman microspectroscopy as medical diagnostic tools has been well demonstrated.[31–35] The main advantages of these techniques are that, they provide a noninvasive, high sensitive label free molecular fingerprint of tissue and cells even in very low sample amounts. The combined application of the Fourier transform infrared (FTIR) and Raman imaging techniques provide consistent and complementary chemical composition and structural information on the same tissue.

In recent years, the pleiotropic and adverse effects of simvastatin on molecular composition and structure of bone[13,14] and muscle[6,7,14] tissues have been studied by our group using FTIR transmission and attenuated total reflectance (ATR)-FTIR spectroscopic techniques. In one of these studies, we reported simvastatin-induced relative protein secondary structural changes on soft tissues (liver, testis, and sciatic nerve) and hard tissues (femur and tibia) by applying neural network approach on well-known amide I protein band (1700 to 1600 cm^{-1}) acquired by ATR-FTIR spectroscopy.[14] Although liver is one of the organs that is mostly affected from drug or chemical treatment,[36–39] simvastatin-liver tissue interaction has not been studied in detail yet. In the current study, besides the accurate determination of protein secondary structure by collecting thousands of the spectra from the sections of a liver using FTIR microscopy, the changes in hepatic lipid composition, the lipid-to-protein ratio and the distribution of saturated and unsaturated hepatic lipids and nucleic acid to protein ratio were determined for the first time, which are important factors for liver disorders. In addition, Raman imaging studies were performed to support FTIR imaging results.

2 Materials and Methods

2.1 *Animal Studies*

Ethical approval was taken from Hacettepe University animal ethical committee. The rats were separated into two groups as control ($n = 5$) and simvastatin-treated ($n = 6$). The control group received serum physiologic solution, while the simvastatin treatment group received simvastatin (50 mg/kg/day) in serum physiologic daily by gavage for 30 days. At the end of the treatment period rats were decapitated and liver samples were taken and stored at −80°C for imaging studies.

2.2 *Sample Preparation*

The frozen tissues were embedded in a tissue freezing medium and were cryosectioned (10-μm thickness) at −20°C. Two adjacent sections for each vibrational techniques per animal were used for infrared and Raman microspectroscopic studies. The sections were transferred onto an IR transparent, 1-mm thick × 13 mm diameter BaF_2 (barium fluoride) infrared windows (Spectral Systems, Hopewell Junction, New York). The samples on BaF_2 windows, were kept at temperature of +4°C in a vacuum desiccator for overnight to remove bulk water from the system. At least two different sections per sample were collected to increase the sample size for chemometric analysis.

2.3 *Data Collection and Spectral Analysis*

2.3.1 *Fourier transform infrared microspectroscopy*

Infrared images and spectra were collected in transmission mode using a Spectrum Spotlight One FTIR spectrometer from PerkinElmer coupled to a Spectrum Spotlight 400 infrared microscope. The microscope is equipped with a liquid nitrogen cooled MCT detector and a CCD camera to provide an optical image of the area under interrogation. FTIR microscope collects IR images of tissue sections by scanning the section pixel by pixel using 25×25 μm pixel size. From these IR images, IR chemical (absorbance) maps were obtained by scanning (pixel size: 6.25×6.25 μm) three different randomly selected regions from each IR image of sections. The size of the spot or pixel was determined by the size of the microscope aperture which may be defined in micrometers. In chemical maps, IR spectra were recorded from each pixel during scanning process. Since the size of the collected IR chemical maps is 400×400 μm^2, a total of 4096 spectra were recorded from each chosen area of each section. Chemical maps were collected in the transmittance mode through the spectral range between 4000 to 700 cm^{-1} with a 4 cm^{-1} resolution and 32 scan numbers. Background spectra were collected for each sample from the free parts (the parts do not contain any sample) of BaF_2 windows.

The resulting FTIR chemical maps were processed using CytoSpec v.2.00.01[40] imaging software package. The bands belong to atmospheric water vapor and tissue freezing medium were removed from raw spectral data. The removal of pixels with too low absorbance values, or with poor signal/noise ratio from the data set in spectroscopic images were also carried out by a quality test [signal-to-noise ratio (S/N) test], since they mainly originate from holes and fissures in tissue sections. For this purpose, in the (S/N) test for biomedical samples, the signal S in each of the 4096 pixels was evaluated as the maximum in the frequency region of the Amide I band (1595 to 1800 cm^{-1}), while the noise N was calculated as the standard deviation in the spectral range 1800 to 1900 cm^{-1} [41]. In order to identify poor quality pixels, those with a S/N smaller than 100 were labeled as bad pixels. The threshold set at 100 was chosen in accordance to Griffiths and De Haseth.[42] All spectra which passed the quality test were subsequently offset corrected and baseline corrected by subtracting a multipoint linear baseline from each spectrum to reduce the spectral variances due to scattering.

Preprocessed spectral data sets were used to obtain average spectra. The average spectra obtained from three randomly-selected regions in each section were compared and found similar indicating the homogeneity of the liver tissue sections. The same procedure was applied for all sections and similar findings were obtained. The IR chemical maps and spectra were imported into ISys (Spectral Dimensions, Olney, Maryland) and OPUS 5.5 software (Bruker Optics, GmbH) and further data analyses were performed using these softwares. Spectral parameters were measured by taking the ratio of the area and intensity values of specific spectral bands, respectively, arisen from proteins, lipids, and nucleic acids.

The integrated spectral regions and baseline points for the infrared bands used in this study are listed in Table 1. The lipid-to-protein ratio was obtained by calculating the ratio of the area of the C—H stretching region to the area under the amide I band. Although the C—H stretching region contains a weak band which mainly originates from proteins (CH_3 symmetric stretching band), the C—H region are generally attributed to mainly lipids.[6,32] The amide I/amide II ratio was calculated by dividing the area under the amide I band to that of amide II band which indicates variation in protein structure.[6,32,38] Nucleic acid to protein ratio was also calculated from the ratios of the band area of specific DNA and/or general nucleic acid band to the area of protein amide II band. FTIR microspectroscopic results were expressed as representative color-coded images for each of these spectral parameters.

Table 1 The spectral regions and baseline points used for particular infrared bands.

Infrared band	Integrated spectral range (cm^{-1})	Baseline points (cm^{-1})
Olefinic=CH	3025 to 3000	3025 to 3000
Total CH	3000 to 2800	3100 to 2750
CH_3 asymmetric stretching	2964 to 2947	3100 to 2750
CH_2 asymmetric stretching	2948 to 2909	3100 to 2750
CH_2 symmetric stretching	2862 to 2849	3100 to 2750
Amide I	1700 to 1590	1780 to 1350
Amide II	1590 to 1500	1780 to 1350

2.3.2 *Raman Microspectroscopy*

Raman spectra were collected using a DXR Raman microscope (Thermo-Fisher, combined with OMNIC Atlus software) equipped with a 780-nm laser providing 14 mW of power on the sample, edge filters, a charge coupled device detector and a 50× objective giving a spot size of 1 μm. The mapping technique was used for the spectra acquisition from an area of 100×100 μm^2 (100 spectra from each area) were collected within a 3200 to 300 cm^{-1} spectral range with two accumulations of 30 s. The spectral preprocessing first was performed to generate Raman scatter spectra alone. The Omnic imaging software automatically corrects for fluorescence interference and cosmic spikes using Cosmic Ray Remover options in spectral software. Although we studied the sample slides on a standard BaF_2 window which has nearly zero background, the micrographs of the BaF_2 were collected as background before sample data acquisition. Raman spectrum of the background was subtracted from each spectrum in order to compensate interfering signals originating from the optical elements in the laser light delivery pathway. Subsequently, spectra with maximum intensities below a threshold were removed from the data set: those spectra corresponded to areas of the sample without tissue.

Raman spectroscopic imaging allowed for building chemical maps based on the intensity of a selected Raman band. Raw Raman spectra were imported into CytoSpec program. A uniform data preprocessing protocol was used for all computational procedures. We have extracted the average spectrum of each map for control and simvastatin-treated spectra. Analyses of the spectra were performed using OPUS 5.5 software (Bruker Optics, GmbH). The spectra were vector normalized with respect to the fingerprint region (1800 to 800 cm^{-1}) which contains the majority of the useful biochemical information. Vector normalization was performed on all spectra to correct intensity

variations for consistency and enable a better comparison of the spectral shapes and relative peak intensities between tissue samples. In this normalization, data for each single spectrum (the absolute intensity values of each wavenumber) were normalized to the total intensity of the same spectrum over the entire spectral region (1800 to 800 cm^{-1}). Vector-normalized intensities of specified bands were used for comparison purpose.[43] Background-corrected and vector-normalized Raman spectra were used for all further analyses.

2.4 *Protein Secondary Structure Analysis*

2.4.1 *Neural network analysis*

Alterations in protein secondary structure were characterized using artificial neural networks (NN) method developed in our laboratory.[44] The NN method was applied to the 1700 to 1600 cm^{-1} spectral region of the FTIR spectra to determine α-helix and total β-sheet content. The details of the method can be found in Severcan et al. [44] This method was successfully applied to biological membranes and tissue proteins to predict the secondary structure of proteins.[32,38,45,46]

2.4.2 *The second derivative intensity calculation*

For the determination of the changes in the protein structure, vector normalized second derivative method was also used. First the second derivative spectra were obtained by applying a Savitzky–Golay algorithm with nine smoothing points. Then, these derivatives were vector normalized at amide I absorption in the 1700 to 1600 cm^{-1} region. The peak intensities were calculated by using the peak minima of the second derivative signals, since they correspond to the peak positions of the original absorption spectra.[6]

2.5 *Principal Component Analysis*

Principal component analysis (PCA) was applied to the vibrational spectra in order to differentiate the groups.[31–35,47–51] The aim of PCA is to reduce the dimensionality of a data set consisting of a large number of interrelated variables, while keeping as much as possible the variation present in the data set. For a vibrational spectral input, this corresponds to the reduction of hundreds of absorbance values at corresponding spectral wavenumbers into a single point. The coordinates are the principal components (PC) and the plot obtained is called the scores plot. The principal components in turn describe the statistical variation in the spectra, i.e., the variability of the spectrum with respect to the mean of the spectra and thus contain the characteristics of the samples.[50,51] Each PC describes the spectral variability among samples in decreasing order. Thus, the first principal component, i.e., PC1, expresses most of the variance in the data; PC2 expresses the second largest variance in the data and so on. As a result, information about the class separation is obtained by clustering the similar samples from the scores plot. An increase in the spatial separation between the two points in a scores plot corresponds to an increase in the dissimilarity between these two samples, i.e., the absorbance spectra in the case of FTIR spectra as the input.[50] The details can be found in Demir et al. [50] PCA was performed on both FTIR and Raman micro spectra using the Unscrambler® X version 10.3 (CAMO) and MATLAB (Mathworks Inc.) programs, respectively. The analyses were performed on absorbance spectra that were vector normalized, seven points smoothed with the Savitzky–Golay algorithm[52] and 2nd degree polynomial baseline corrected. Normalization, smoothing and baseline correction were performed using the OPUS 5.5 software (Bruker Optics, GmbH).

PCA was applied to different regions of the FTIR and Raman spectra for the control and simvastatin-treated groups and the regions that revealed best discriminations of the groups were determined.

2.6 *Statistics*

The results were expressed as means ± standard error of mean for each group. The differences in the means of the groups were compared by Student t-test using the Minitab Statistical Software Release 3.0 program (State College, Pennsylvania); p values equal to or less than 0.05 were accepted as significantly different from the control group. The degree of significance was denoted as $p < 0.05*$, $p < 0.01**$, $p < 0.001**$

3 Results and Discussion

In the current study, simvastatin-liver tissue interaction in terms of compositional and structural properties was studied using FTIR and Raman imaging techniques. In humans, 80 mg day^{-1} of simvastatin is the highest recommended dose for treatment of hypercholesterolemia. For an individual who weighs 70 kg, this dose corresponds to 1.1 mg/kg.[53]

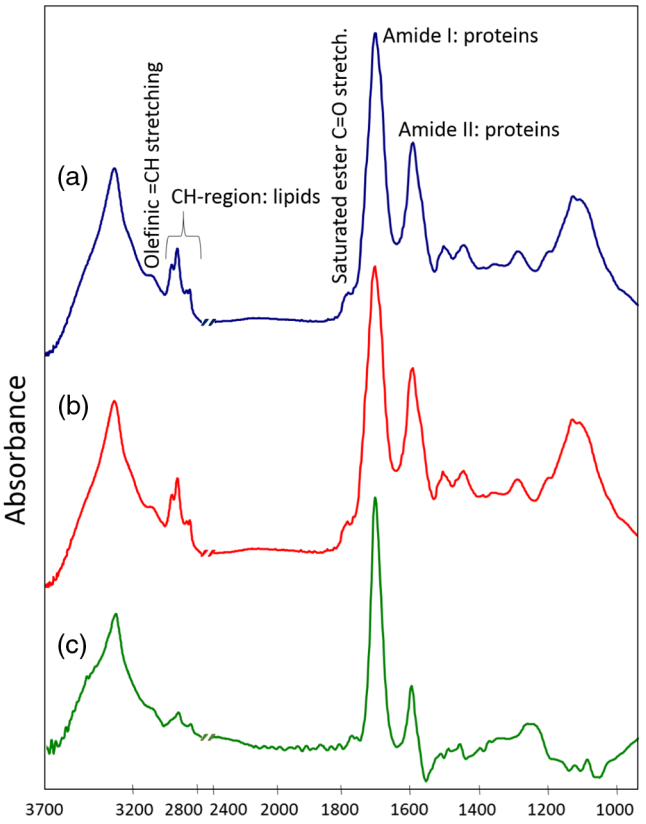

Fig. 1 Mean spectra of (a) control, (b) simvastatin-treated liver tissues, and (c) the difference spectrum between the means (control-treated) 3700 to 850 cm^{-1} region. A Student t-test was performed for comparisons. Simvastatin-induced changes in the calculated ratios of these bands are presented in Table 3 and FTIR images in Fig. 2.

Pharmacokinetic studies in animals showed that higher statin doses are required for animals to access similar effective doses in humans.[54] For animal studies, high oral dose simvastatin corresponds to 50 to 100 mg/kg/day.[55,56] In this study, simvastatin dose (50 mg/kg/day) was chosen according to previous animal studies including rat.[56]

3.1 *Fourier Transform Infrared Microspectroscopy*

Figure 1 shows the average FTIR spectra of control and simvastatin-treated liver tissues and their difference spectrum in the 3700 to 850 cm^{-1} region. The detailed spectral band assignments are given in Table 2.

Since we aimed to study the tissue samples in the environment that is close to natural *state*, the bound water was not removed from the system by applying very heavy drying process. Instead, we applied mild vacuum drying for overnight to tissue sections to keep the bound water in the system but only remove bulk water. This is clearly seen from Fig. 1 that, the spectrum does not contain bulk water located around 2100 cm^{-1}. However, the bound water located around 3500 cm^{-1} can be seen as a shoulder in Fig. 1.

As seen from the difference spectrum, there are significant changes in several bands due to the simvastatin treatment. Simvastatin-induced changes in IR band area ratio for the control and simvastatin-treated livers are presented in Table 3. The band area ratios were calculated as mentioned in the Sec. 2. Representative FTIR chemical maps of specific band ratios for the control and simvastatin-treated liver tissues are presented in Figs. 2(a)–2(c). The variations in the area under the spectral bands give information about concentration of the functional groups belonging to the relevant molecules; for example, the increase in the band area values represents an increase in the concentration of assigned molecules.[32,38]

In order to determine the level of saturation, the main lipid bands in the 3000 to 2800 cm^{-1} region of infrared spectra was used. The ratio of saturated lipids (CH_2 antisymmetric + CH_2 symmetric) to unsaturated lipids (olefinic=CH) was found to be higher in the simvastatin-treated liver tissue [Fig. 2(a) and Table 3]. The olefinic=CH stretching mode of the HC=CH groups can be used to probe lipid peroxidation as a measure of unsaturation in the acyl chains.[6,7,38,57,58] This increase in the mentioned ratio indicates a pronounced decrease in the amount of unsaturated lipids in comparison to the saturated ones. This is because simvastatin treatment also induces a decrease in the area of saturated lipids as seen from Table 3. Supporting our results, in a recent study, a decrease in the intensity of olefinic band was attributed to a decrease in unsaturation indicating lipid peroxidation in the hippocampus of mice with Alzheimer's disease.[58] In addition, the other simvastatin study[7] also reported a significant increase in this ratio for the simvastatin-treated extensor digitorum longus (EDL) muscles compared to the controls, supporting the results of the current study. The statins, including simvastatin, caused hemototoxicity in rat hepatocytes in which significant amount of lipid

Table 2 Band assignments of major absorptions in IR spectrum of control liver tissue in the 4000 to 800 cm^{-1} region.

Wavenumber (cm^{-1})	Definition of the spectral assignment
3500 3292	Bound water Amide A: mainly N–H stretching of proteins
3077	Amide B: N–H stretching of proteins
3012	Olefinic=CH stretching vibration: unsaturated lipids, cholesterol esters
2958	CH_3 asymmetric stretch: mainly proteins
2925	CH_2 asymmetric stretch: mainly lipids
2872	CH_3 symmetric stretch: mainly proteins
2853	CH_2 symmetric stretch: mainly lipids
1732	Saturated ester C=O stretch: phospholipids, triacylglycerols, cholesterol esters
1653	Amide I: protein (80% C=O stretching, 10% N–H bending, 10% C–N stretching)
1544	Amide II: protein (60% N–H bending, 40% C–N stretching)
1455	CH_2 bending: mainly lipids, protein
1396	COO^- symmetric stretch: fatty acids and amino acids
1310	Protein (amide III)
1239	PO_2^- asymmetric stretch: nucleic acids, phospholipids
1152	CO–O–C asymmetric stretching: glycogen and nucleic acids
1080	PO_2^- symmetric stretch: mainly nucleic acids, phospholipids,
1052	Glycogen
1040	C–O stretching: polysaccharides, glycogen
890	DNA

Table 3 The IR band area ratios of some functional groups for the control and simvastatin-treated livers.

Band Ratio	Control ($n = 5$)	Simvastatin ($n = 6$)
CH_2 antisym + CH_2 sym/olefinic	2.820 ± 0.120	3.210 ± 0.160[a]
Total C–H/Amide I	0.212 ± 0.001	0.220 ± 0.002[b]
CH_2 antisym/Amide I	0.098 ± 0.001	0.101 ± 0.001[a]
C=O stretching/Amide I	0.032 ± 0.001	0.064 ± 0.001[a]
Amide I/Amide II	1.990 ± 0.010	1.960 ± 0.010[b]
PO_2^- sym/Amide II	0.703 ± 0.050	0.986 ± 0.090[b]
DNA ($890\ cm^{-1}$)/Amide II	0.212 ± 0.035	0.326 ± 0.065[a]
DNA ($890\ cm^{-1}$)/PO_2^- sym	0.301 ± 0.030	0.331 ± 0.045

Note: The values are the mean ± standard error of mean for each group. Comparison was performed by the *t*-test.
[a]The degree of significance was denoted as: $p < 0.05$.
[b]The degree of significance was denoted as: $p < 0.01$.

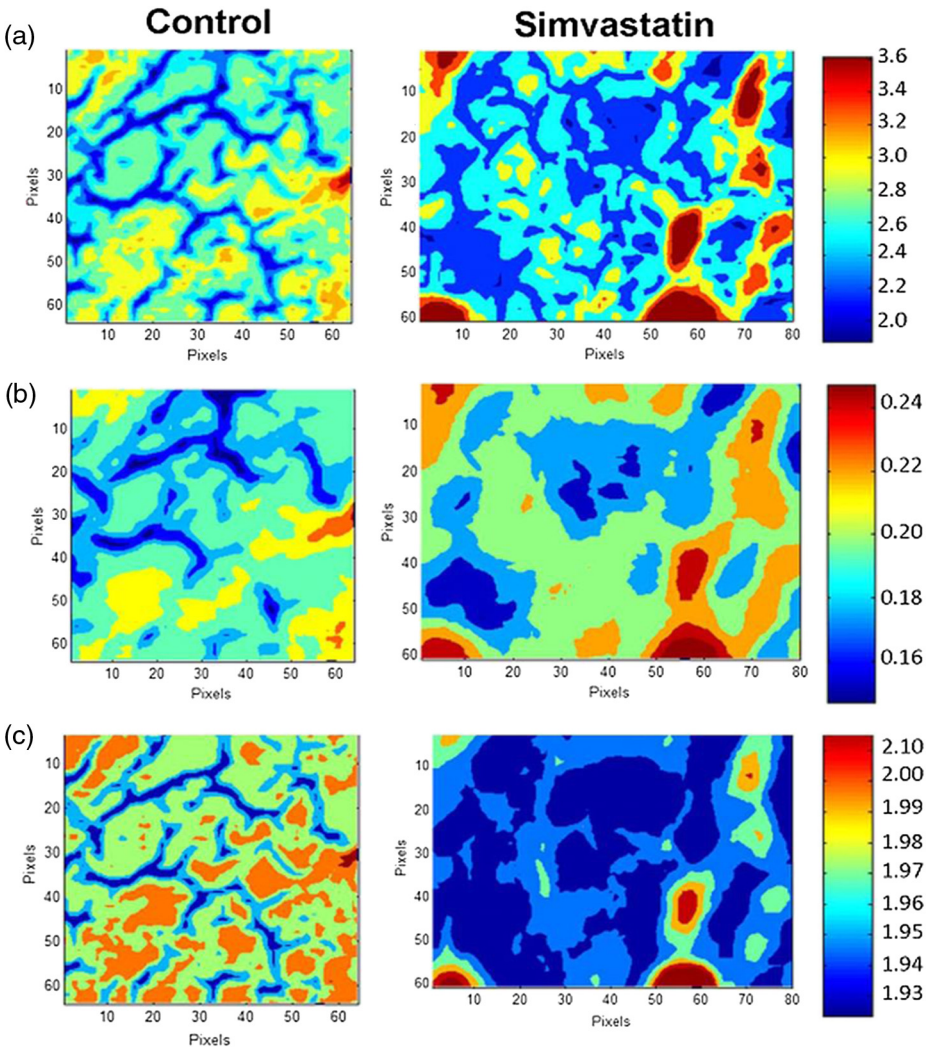

Fig. 2 Representative FTIR images for (a) CH_2 antisymmetric + CH_2 symmetric/olefinic; (b) total C—H/Amide I; and (c) amide I/amide II ratios for the control and simvastatin-treated liver tissues.

peroxidation was observed.[59] That study reported that the adverse effect of statins in hepatocytes is mediated through oxidative stress.

The lipid-to-protein ratio was obtained by calculating the ratio of the total area of the C—H stretching region to the area under the amide I band. It was visually apparent from the Fig. 2(b) that the value of lipid/protein ratio increased for the simvastatin-treated liver tissue compared with the control. This is due to the decrease in the protein amount. Indeed, in simvastatin-treated group, we found a significant decrease in the amount of total protein content compared to the control [from 0.89 to 0.80 for amide I ($p < 0.01$) and from 0.45 to 0.41 for amide II ($p < 0.01$)] by monitoring the area under the protein bands (amide I and amide II). This result was supported by the decrease in the area ratio of amide I/amide I + amide II. As can be seen from Table 2, the increased band area ratio of CH_2 antisymmetric to amide I also supported our findings. Another supporting result for the increase in lipid/protein ratio was obtained by taking the ratio of the band areas of saturated ester C=O stretching band to amide I band (Table 3). A similar increase in lipid-to-protein ratio was also reported in simvastatin-treated bone and EDL muscle,[7,14] suggesting that there was a much more pronounced decrease in protein content when compared with those of lipid content.[7] Vaghasija et al. investigated the hepatotoxicity induced by simvastatin treatment in rats.[60] The authors reported that simvastatin treatment significantly decreased the liver tissue levels of reduced glutathione, super oxide dismutase and catalase in treated rats compared to the control group. It was also reported that drug treatment decreased the total protein levels and caused depletion of proteins indicating simvastatin-induced oxidative stress mediated hepatotoxicity.[60] The decrease in liver total protein content, in the current study, may be due to the oxidative stress mediated hepatotoxicity in simvastatin-treated group.

The bands located at 1653 and 1544 cm^{-1} are assigned to amide I and amide II vibrational modes of structural proteins, respectively. The amide I absorption band, arises mainly from the C=O stretching vibration with minor contributions from the out-of-phase CN stretching vibration, the CCN deformation and the NH in-plane bending. The amide II mode is the out-of-phase combination of the NH in plane bending and the CN stretching vibrations with smaller contributions from the CO in plane bending and the NC stretching vibrations.[37] Therefore, the changes in the band areas of amide I and amide II reflect an alteration in the protein structure in tissues.[6,32,37] As seen from Fig. 2(c) and Table 3, there was a significant decrease ($p < 0.01$)

in the area ratio of the amide I to amide II bands in the simvastatin group, implying a change in protein structure in simvastatin treated liver.[6]

In order to better understand and comment on the changes in protein secondary structure, neural network method was used.[44] The results are presented in Table 4(a). NN results revealed a significant decrease in α-helix ($p < 0.01$) and an increase in total β-sheet and random coil ($p < 0.05$) content in simvastatin-treated group with respect to the control group. Our previous study reported the similar type of variations in the protein secondary structure which were induced by 50 mg/kg/day simvastatin therapy in soft (liver, testis and sciatic nerve) and hard tissues (femur and tibia), using ATR-FTIR spectroscopy coupled with NN method.[14] ATR-FTIR spectroscopy gives valuable relative information about protein secondary structure; however, in this technique, randomly selected portions of the homogenous tissues are investigated, whereas in the current study, average FTIR spectrum is obtained from thousands of spectra obtained from the tissue slices for each sample. Therefore, FTIR imaging technique provided more reliable relative information about protein secondary structure.[24] The neural network gives us the total amount of each secondary structural parameter. Therefore, the β-sheet results include the sum of native β-sheet, anti-parallel β-sheet and aggregated β-sheet content. For further investigation of the contribution of each β-sheet structural content, the relative changes in the protein structure were determined from the intensities of the sub-bands in the second derivative of the amide I band (Fig. 3). The intensity values of these bands in liver tissues of the control and simvastatin-treated groups are listed in Table 4(b). As seen from the table, although, there is no significant change in the native β-sheet band at 1638 cm^{-1}, the antiparallel β-sheet at 1690 cm^{-1} and aggregated β-sheet at 1629 cm^{-1} significantly increased in the simvastatin group when compared to the control group. The peak at 1659 cm^{-1} that is due to α-helical structure, significantly decreased in the treated group as in agreement with in the NN results. Supporting NN results, the random coil structure peak at 1648 cm^{-1} also significantly increased in the simvastatin-treated group compared to the control. The second derivative intensity calculation studies showed that the increase in β-sheet content obtained from NN study, was due to the increase in anti-parallel and aggregated β-sheets. In the current study, the decrease in α-helix, and the increase in random coil and aggregated β-sheet structures imply simvastatin-induced protein denaturation in liver tissues.[14] Our results clearly show that

Table 4 The protein secondary structure content of the control and simvastatin-treated livers based on FTIR data in the 1600 to 1700 cm^{-1} spectral region (amide I band). The results of the neural network predictions (A), the intensities of the sub-bands in the second derivative (B) of the amide I band.

Functional Groups	Control ($n = 5$)	Simvastatin ($n = 6$)
(a)	**Neural network predictions (NN)**	
α-helix	46.94 ± 0.80	43.65 ± 1.00^{b}
β-sheet	19.06 ± 0.90	20.24 ± 1.10
Random coil	14.80 ± 0.75	16.40 ± 0.40^{a}
(b)	**Second derivative intensities**	
α-helix	0.174 ± 0.010	0.132 ± 0.015^{c}
β-sheet	0.106 ± 0.008	0.100 ± 0.010
Anti-parallel β-sheet	0.080 ± 0.006	0.110 ± 0.010^{b}
Aggregated β-sheet	0.135 ± 0.008	0.156 ± 0.006^{b}
Random coil	0.090 ± 0.004	0.099 ± 0.004^{a}

Note: The values are the mean $\pm$ standard error of mean for each group. Comparison was performed by the t-test.
[a]The degree of significance was denoted as: $p < 0.05$.
[b]The degree of significance was denoted as: $p < 0.01$.
[c]The degree of significance was denoted as: $p < 0.001$.

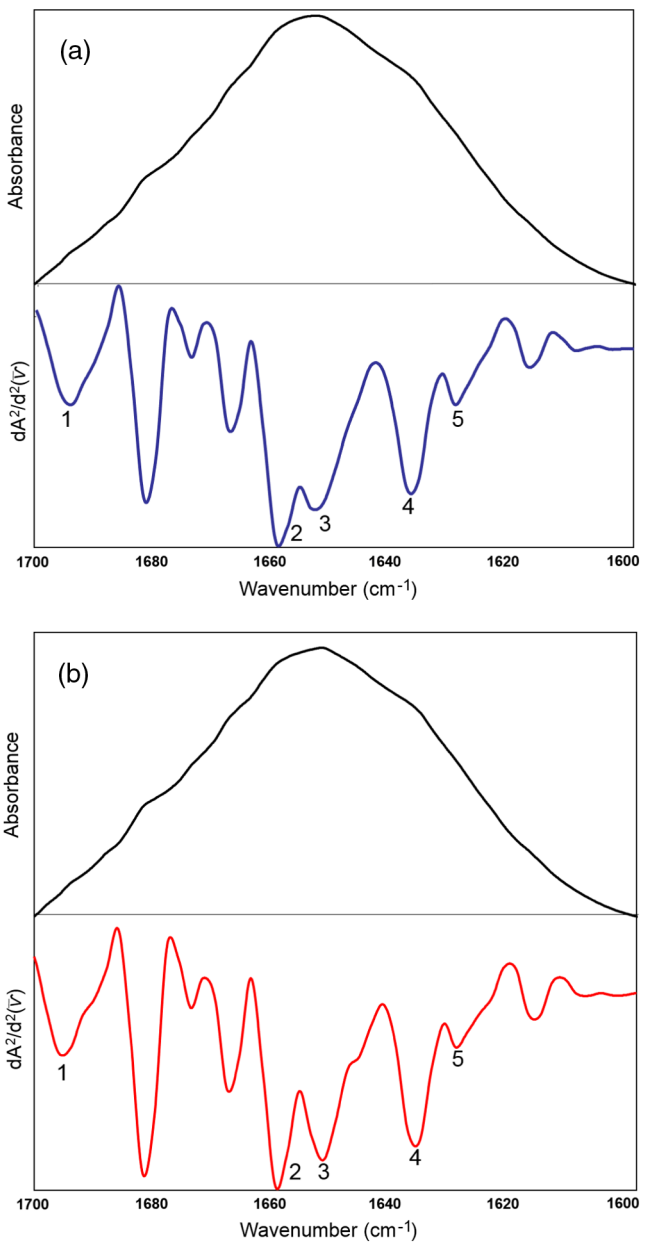

Fig. 3 The average absorbance and second derivative spectra of control (a) and treated (b) groups in 1700 to 1600 cm^{-1} region. The numbers represent secondary structure bands under amide I band [1: antiparallel β-sheet; 2: alpha-helix; 3: random coil; 4: native β-sheet; and 5: aggregated β-sheet structure].

protein secondary structure is significantly affected from simvastatin treatment. It is worth noting that the same type of behavior such as a decrease in α-helix and an increase in total β-sheet is almost a general trend at the early stage of several diseases such as diabetes[32,61] and neurodegenerative diseases.[62]

The band at 1080 cm^{-1} is due to symmetric stretching vibrations of PO_2^- groups (mainly nucleic acids). The area ratios of the 1080 to 1550 cm^{-1} (amide II; protein) bands could be used to probe nucleic acids in the tissues.[63,64] This ratio is generally used for identifying cancer tissues and normal tissues.[63,64] In the current study, this ratio increased in the treated tissues compared to the controls implying a simvastatin-induced increase in nucleic acid levels in the treated tissues. The band at 890 cm^{-1} due to the deoxyribose ring vibrations, is a specific DNA band and can be used to probe DNA content.[65] The ratio of the DNA band area to protein (amide II at 1550 cm^{-1}) or phosphate (1080 cm^{-1}) band areas were also calculated and found to be increased in the simvastatin treated liver tissues when compared to the control livers implying an increase in DNA content (Table 2). It was previously reported that oxidative stress can trigger cell-cycle arrest and lead to an increase of mitochondrial mass and mitochondrial DNA (mtDNA) in human cells.[66] The alteration of mitochondrial mass and mtDNA in cells might be uncoupled from the cell-cycle-controlled biosynthesis of chromosomal DNA. In the study of Lee et al. [66] MRC-5 cells were treated with a statin called lovastatin and it was observed that statin drug caused cell-cycle arrest and induced an increase in mtDNA content. These results imply that the increase in mitochondrial mass and mtDNA content are the early molecular events of human cells in response to endogenous or exogenous oxidative stress through cell-cycle arrest.[66]

3.2 *Raman Microspectroscopy*

The average Raman spectrum of a normal liver rat tissue in the 1800 to 800 cm^{-1} fingerprint region is shown in Fig. 4. In this region, a Raman spectrum of a tissue is dominated by a number of vibrational modes of biomolecules, such as proteins, lipids, and nucleic acids. The tentative assignments of major bands in Raman spectrum is given in Table 5.

Raman spectra allow assessment of the overall molecular constitution of biological samples, based on specific signals from proteins, nucleic acids, lipids, and carbohydrates. Simple but effective diagnostic algorithms have been proposed on the basis of the empirical analysis of Raman spectra in terms of peak intensity or peak intensity ratio measurements and have been used to differentiate normal and diseased tissues as well as different chemical state of organs and cells.[31,67–71]

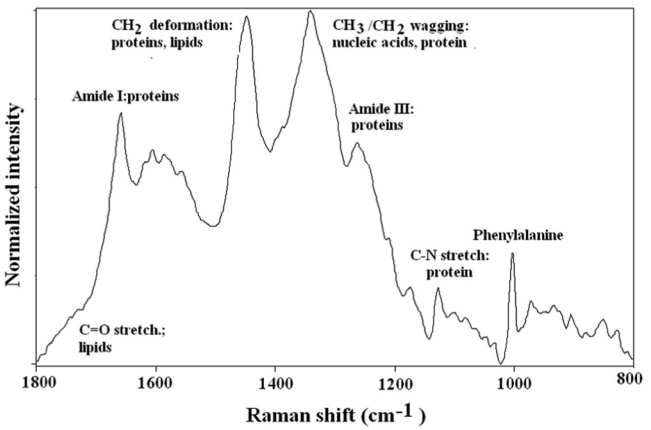

Fig. 4 The average Raman spectrum of normal liver rat tissue in the 1800 to 800 cm^{-1} fingerprint region.

In the present study, the differences observed in the peak intensities or ratio of peak intensities of Raman bands were used to characterize normal and simvastatin-treated liver tissues. Representative Raman images based on the intensity distribution of the amide I band for the control and simvastatin-treated liver tissues are shown in Figs. 5(a) and 5(b), respectively. As seen from the Fig. 5, the intensity of amide I band decreased in the simvastatin treated group as supporting the infrared data.

The calculated Raman intensity ratios of selected main bands in the finger print region indicated the spectral changes between the normal and treated tissues (Table 6). The lipid bands that were used in FTIR imaging studies in the 3000 to 2800 cm^{-1} region have not been used in Raman spectra due to the strong fluorescence and scattering influence. Therefore, in order to obtain information about lipids, the bands at 1743 and 1446 cm^{-1} were investigated. The former band is attributed to the C=O stretching vibrations from the ester bonds between

Table 5 The peak positions and general band assignments in a Raman spectrum of control liver tissue in the 1800 – 800 cm^{-1} region.

Wavenumber (cm^{-1})	Definition of the spectral assignment
1743	ν (C=O) stretching (lipids)
1657	ν (C=O), Amide I
1603	C=C stretching
1556	Amide II
1446	CH_2 deformation mode of lipids (mainly) and proteins
1387	CH_2 and CH_3 symmetric deformation of proteins
1339	CH_3/CH_2 wagging (nucleic acids, protein)
1261	Amide III (C–N stretching mode of proteins, indicating mainly α-helix conformation),
1209	Tryptophan and phenylalanine
1172	δ(C–H), tyrosine
1127	C–N stretch,protein
1102	Phospholipids, proteins
1082	PO_2^-, nucleic acid
1002	Phenylalanine aromatic amino acids-symmetric ring breathing mode
972	C–C backbone
933	C–C stretching mode of proline, valine, and protein backbone
880	Lipid, hydroxyproline
854	Tyrosine and C–C stretching vibrations of proline
829	O–P–O, DNA

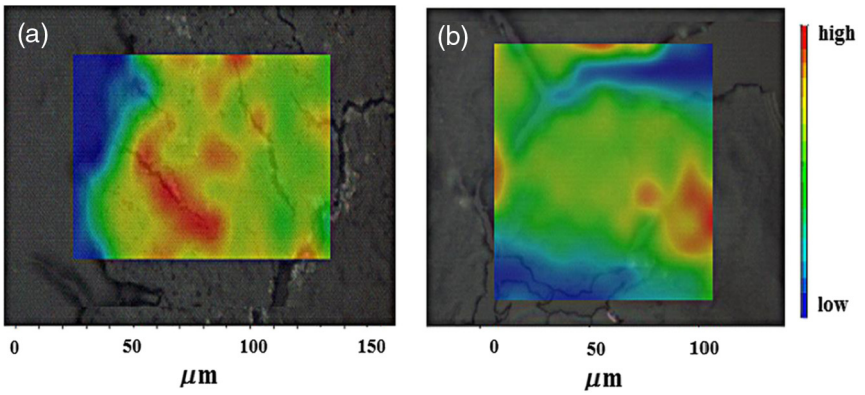

Fig. 5 Raman chemical images based on Amide I intensity overlaid of the optical images of the (a) control and (b) simvastatin treated liver tissues. Color bar: low intensity (blue), high intensity (red).

Table 6 Raman band intensity ratios for the control and simvastatin-treated liver tissues.

Functional group	Control ($n = 5$)	Simvastatin ($n = 6$)
Lipid/Amide I (I_{1743}/I_{1657})	0.169 ± 0.004	0.189 ± 0.012^{b}
Lipid/Amide I (I_{1446}/I_{1657})	1.339 ± 0.015	1.392 ± 0.041^{b}
PO_2^-/Amide II (I_{1082}/I_{1556})	1.314 ± 0.040	1.674 ± 0.015^{b}
DNA/Amide II (I_{827}/I_{1556})	1.816 ± 0.045	2.003 ± 0.075^{a}
DNA/PO_2^- (I_{827}/I_{1082})	1.369 ± 0.035	1.402 ± 0.030^{a}

The values are the mean ± standard error of mean for each group. Comparison was performed by the *t*-test.
[a]The degree of significance was denoted as: $p < 0.05$.
[b]The degree of significance was denoted as: $p < 0.01$.

glycerol and the fatty acids.[72] This band was used to get information about simvastatin-induced variations in the lipid-to-protein ratio. The increase in the intensity ratio of 1743 cm^{-1} (lipid) to 1657 cm^{-1} (amide I) indicated a decrease in the level of lipid content as supporting FTIR studies. Since there was a much more pronounced decrease in protein content when compared with the lipid content (according to FTIR microspectroscopy studies), this result also supported simvastatin-induced decrease in protein and lipid contents in the treated tissues.

The ratio of band intensities of CH_2 bending (mainly lipids) at 1446 cm^{-1} to amide I (protein) at 1657 cm^{-1} was also calculated since these bands are sensitive to histological abnormality[67] and has been used in previous studies for separating tumors from normal tissues spectrally in the brain, breast, colon cervix, and the lung.[67,70,71,73,74] Supporting FTIR studies, this ratio also increased in the simvastatin-treated tissue with respect to the normal liver tissue.

The band at 1082 cm^{-1} [the symmetrical stretching vibrations of the phosphodioxy (PO_2) moiety] is used as representative of nucleic acid content in tissue.[75–77] The band at 829 cm^{-1} is considered as one of the DNA conformational marker bands (O—P—O).[76]

In the current study the intensity ratios of the PO_2^- to protein (amide II at 1556 cm^{-1}) bands and DNA to protein (amide II) or phosphate bands were also calculated. Similar to the FTIR imaging studies, these ratios significantly increased in the simvastatin treated tissues compared to the controls implying an increase in nucleic acid levels and DNA content (Table 6). The increase in the DNA content may be due to the simvastatin induced-oxidative stress.

3.3 *Principal Component Analysis*

To differentiate the control and simvastatin-treated groups based on the molecular alterations from the vibrational spectra, PCA was applied to the different spectral regions of vibrational spectra. Best results were obtained for the protein (amide II) region (1600 to 1480 cm^{-1}) and lipid (triglyceride/cholesterol ester) region (1780 to 1700 cm^{-1}) for IR, and for the whole region (3400 to 300 cm^{-1}) for Raman spectroscopy. The results of PCA performed on the vector normalized spectra of control and simvastatin-treated groups can be seen in Figs. 6 and 7 for infrared and Raman spectra, respectively. As can be seen from the figures, both vibrational spectroscopic techniques successfully differentiated the drug-treated group from the control group in the regions that were used.

PCA analyses were performed on the average spectra of each chemical map from each sample. As mentioned in FTIR studies section, three chemical maps were recorded from three different randomly-selected regions of each sample section. Thus, PCA was performed by using 15 spectra for control (three average spectra × five samples) and 18 spectra for drug-treated (three average spectra × six samples) groups as seen in Fig. 6. Since the number of samples used in the PCA was quite small, some form of validation had to be used so that the PCA model obtained can be used for the new samples to be tested. In such cases it is best to use leave-one-out type cross validation. For all the PCA performed in this work, full cross validation (i.e., leave-one-out validation) was used. The score plots obtained from the calibration set and the cross validation set were compared so that prediction errors are kept at a minimum level.

Figure 6(a) shows the scatter plot (PC2 versus PC1) of the scores obtained from the PCA of amide II region (1600 to 1480 cm^{-1}) of the IR spectral region. As can be seen from the figure, the first PC score (PC1) corresponds to 95% variability and the second PC (PC2) corresponds to 4% variability. While the PC2 for the control group is mostly greater than or equal to zero, it becomes less than or equal to zero for the simvastatin treated group indicating clear distinction between the two groups. Out of the 15 control spectra only for two

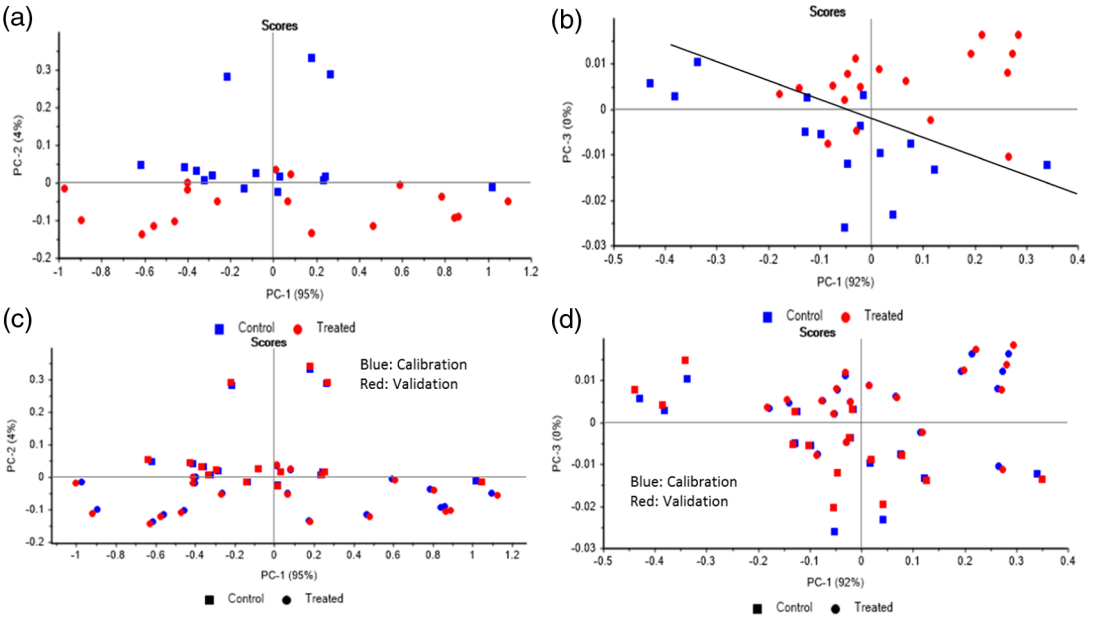

Fig. 6 (a) PCA scatter plots, (b) leave-one-out cross validation, for FTIR spectral region of 1600 to 1480 cm^{-1}. (c) PCA scatter plots and (d) leave-one-out cross validation, for FTIR spectral region of 1780 to 1700 cm^{-1}.

spectra PC2 < 0, and out of 18 treated spectra only two spectra have PC2 > 0. Fig. 6(b) shows the PCA result obtained from the calibration set (blue) and the scores corresponding to leave-one-out cross validation (red) for each sample. As seen from the figures the calibration and cross validation results are very close to each other and therefore the PCA model obtained is reliable.

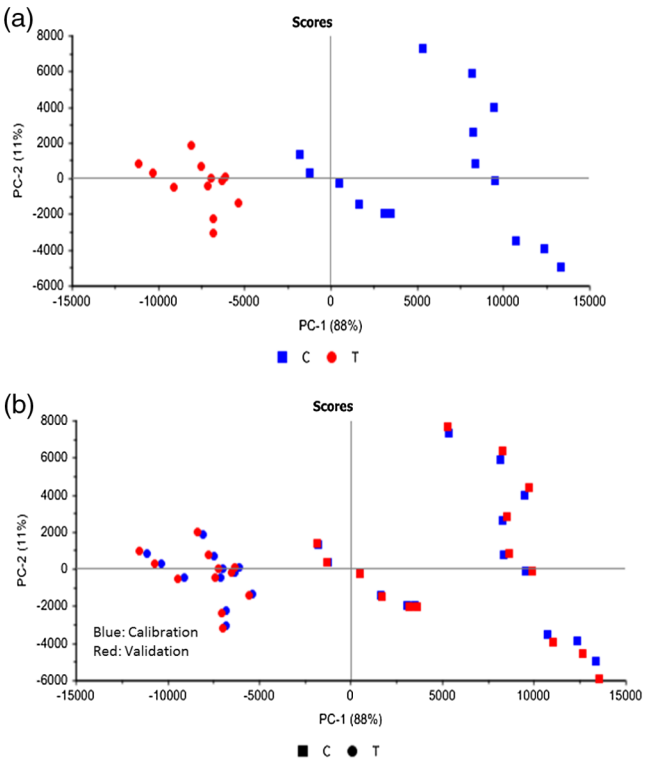

Fig. 7 (a) PCA scatter plots and (b) leave-one-out cross validation, for the whole Raman spectral region (3400 to 300 cm^{-1}).

Figures 6(c) and 6(d) are similar plots for the IR spectral region of 1780 − 1700 cm^{-1}. In this case, the discrimination between the control and simvastatin treated groups were observed in the PC3 versus PC1 plots where PC1 has a variability of 92% and PC3 has a variability less than 1%. This result is expectable because the discrimination is due to a narrow lipid peak overlapped by the broad amide I band.

To assess the capability of Raman spectra to differentiate simvastatin-treated tissue samples from the control tissue samples, PCA analysis were performed on the average spectra of Raman chemical map of each sample of the Raman signal. For the PCA analysis of Raman spectra, 15 spectra were obtained from 5 control samples and 12 spectra were obtained from 6 drug-treated samples. PCA results using leave-one-out cross validation for the whole region (3200 to 300 cm^{-1}) can be seen in Fig. 7(a). The score plot PC1 versus PC2 shows a distinct clustering of the two groups. Figure 7(b) shows the score plots for the calibration set (blue) and the scores for leave-one-out validation for each spectrum (red).

4 Concluding Remarks

In recent years, spectral histopathology has become practical and preferable tool to obtain morphological information, which is commonly used in classical cytopathology and histopathology for early diagnosis of diseases. Spatially resolved spectroscopic images provide the distribution of biochemical components (proteins, lipids, DNA) within a tissue section without the use of stains or probes. In this work, we investigated the effects of high dose simvastatin treatment on liver tissues of healthy rats using infrared and Raman images acquired by FTIR and Raman microspectroscopy, respectively. The current results revealed that high dose simvastatin induces significant variations in the content of lipids, proteins and nucleic acids. The ratio values of these components derived from FTIR and Raman microspectra indicate lipid peroxidation, increase in mtDNA content and depletion of proteins in drug-treated

liver tissues implying oxidative stress mediated hepatotoxicity induced by simvastatin. Furthermore, protein secondary structure predicted by NN and also calculated from second derivative intensities, revealed a significant decrease in α-helical and native β-sheet content while there was an increase in antiparallel and aggregated β-sheet structure and random coil content in the simvastatin treated group. These results indicate high dose simvastatin-induced protein denaturation. Finally, the control and simvastatin-treated group were successfully discriminated by using PCA method.

This study demonstrated the complementary feature of Raman and FTIR microspectroscopy techniques for effective characterization and detection of spectral differences between the normal and drug-treated tissues by revealing the adverse effect of simvastatin on the macromolecules of liver tissues in terms of structural parameters which are important factors for liver disorders.

Acknowledgments

S.Bayarı would like to thank the Higher Education Council of Turkey for the fellowship to visit Igor Lednev lab to perform Raman imaging studies. We thank Dr. Alexander Rzhevskii and Thermo Fisher Scientific Inc. for their advisement and expertise and access to their DXR Raman microscope.

References

1. A. Corsini, F. M. Maggi, and A. L. Catapano, "Pharmacology of competitive inhibitors of HMG-CoA reductase," *Pharmacol. Res.* **31**, 9–27 (1995).
2. D. J. Maron, S. Fazio, and M. F. Linton, "Current perspectives on statins," *Circulation* **101**, 207–213 (2000).
3. S. Iseri et al., "Simvastatin attenuates cisplatin-induced kidney and liver damage in rats," *Toxicology* **230**, 256–264 (2007).
4. B. Hajipour et al., "Anti-oxidative effect of simvastatin in liver and lung tissue after hepatic ischemia/reperfusion in rat," *J. Med. Sci.* **10**, 66–70 (2010).
5. H. Bays and E.A. Stein, "Pharmacotherapy for dyslipidaemia-current therapies and future agents," *Expert Opin. Pharmacother.* **4**, 1901–1938 (2003).
6. N. Simsek Ozek et al., "Low dose simvastatin induces compositional, structural and dynamic changes in rat skeletal extensor digitorum longus muscle tissue," *Biosci. Rep.* **30**, 41–50 (2010).
7. N. Simsek Ozek et al., "Structural and functional characterization of simvastatin-induced myotoxicity in different skeletal muscles," *Biochim. Biophy. Acta* **1840**, 406–415 (2014).
8. M. Krishan, "Best-selling human medicines 2002–2004 (editorial)," *Drug Discovery Today* **10**, 739–742 (2005).
9. R. Krysiak, W. Zmuda, and B. Okopien, "The effect of simvastatin-ezetimibe combination therapy on adipose tissue hormones and systemic inflammation in patients with isolated hypercholesterolemia," *Cardiovasc. Ther.* **32**, 40–46 (2014).
10. E. Barone, F. Di Domenico, and D. A. Butterfield, "Statins more than cholesterol lowering agents in Alzheimer disease: their pleiotropic functions as potential therapeutic targets," *Biochem. Pharmacol.* **88**, 605–616 (2014).
11. M. Zhu et al., "Upregulation of protein phosphatase 2A and NR3A-pleiotropic effect of simvastatin on ischemic stroke rats," *PLoS One* **7**, e51552 (2012).
12. N.A. Salem, N. Assaf, and H.H. Ahmed, "Pleiotropic effects of rimonabant and simvastatin on obesity associated multiple metabolic risk factors in rats," *Eur. Rev. Med. Pharmacol. Sci.* **16**, 797–807 (2012).
13. S. Garip and F. Severcan, "Determination of simvastatin-induced changes in bone composition and structure by Fourier transform infrared spectroscopy in rat animal model," *J. Pharm. Biomed. Anal.* **52**, 580–588 (2010).
14. S. Garip et al., "Evaluation and discrimination of simvastatin-induced structural alterations in proteins of different rat tissues by FTIR spectroscopy and neural network analysis," *Analyst* **135**, 3233–3241 (2010).
15. J. Beltowski, G. Wojcicka, and A. Jamroz-Wisniewska, "Adverse effects of statins—mechanisms and consequences," *Curr. Drug* **4**, 209–228 (2009).
16. M. Evans and A. Rees, "The myotoxicity of statins," *Curr. Opin. Lipidol.* **13**, 415–420 (2002).
17. P. Gazzerro et al., "Pharmacological actions of statins: a critical appraisal in the management of cancer," *Pharmacol. Rev.* **64**, 102–104 (2012).
18. V. Z. Lankin et al., "Antioxidants decreases the intensification of low density lipoprotein in vivo peroxidation during therapy with statins," *Mol. Cell. Biochem.* **249**, 129–140 (2003).
19. N. A. Le et al., "Changes in lipoprotein particle number with ezetimibe/simvastatin coadministered with extended-release niacin in hyperlipidemic patients," *J. Am. Heart Assoc.* **2**, e000037 (2013).
20. X. Song et al., "1H NMR-based metabolomics approach to evaluate the effect of Xue-Fu-Zhu-Yu decoction on hyperlipidemia rats induced by high-fat diet," *J. Pharm. Biomed. Anal.* **78**, 202–210 (2013).
21. P. P Toth et al., "Niacin extended-release/simvastatin combination therapy produces larger favorable changes in high-density lipoprotein particles than atorvastatin monotherapy," *Vasc. Health Risk Manage* **8**, 39–44 (2012).
22. W. J Insull et al., "Combination of niacin extended-release and simvastatin results in a less atherogenic lipid profile than atorvastatin monotherapy," *Vasc. Health Risk Manage* **6**, 1065–1075 (2010).
23. L. Le Moyec et al., "Serum 1H-nuclear magnetic spectroscopy followed by principal component analysis and hierarchical clusteranalysis to demonstrate effects of statins on hyperlipidemic patients," *NMR Biomed.* **18**(7), 421–429 (2005).
24. Y. Sun et al., "Beneficial effects of cordycepin on metabolic profiles of liver and plasma from hyperlipidemic hamsters," *J. Asian Nat. Prod. Res.* **13**(6), 534–46 (2011).
25. H.-J Yang et al., "An effective assessment of simvastatin-induced toxicity with NMR-based metabonomics approach," *PLoS One* **6**(2), e16641 (2011).
26. J. C. Chatham and S. J. Blackband, "Nuclear magnetic resonance spectroscopy and imaging in animal research," *ILAR J.* **42**(3), 189–208 (2001).
27. F. Borthwick et al., "Simvastatin treatment upregulates intestinal lipid secretion pathways in a rodent model of the metabolic syndrome," *Atherosclerosis* **232**(1), 141–148 (2014).
28. Y. E. Cho et al., "Integrative analysis of proteomic and transcriptomic data for identification of pathways related tosimvastatin-induced hepatotoxicity," *Proteomics* **13**(8), 1257–1275 (2013).
29. E. van der Meij et al., "A clinical evaluation of statin pleiotropy: statins selectively and dose-dependently reduce vascular inflammation," *PLoS One* **8**(1), e53882 (2013).
30. S. Garip et al., "Epileptic seizure-induced structural and functional changes in rat femur and tibia bone tissues: a Fourier transform infrared imaging study," *J. Biomed. Opt.* **18**(11), 111409 (2013).
31. C. Krafft et al., "Crisp and soft multivariate methods visualize individual cell nuclei in Raman images of normal liver tissue sections," *Vib. Spectrosc.* **55**, 90–100 (2011).
32. Ö. Bozkurt et al., "Structural alterations in rat liver proteins due to STZ-induced diabetes and the recovery effect of selenium: an FTIR microspectroscopy and neural network study," *J. Biomed. Opt.* **17**, 076023 (2012).
33. G. McLaughlin, K. C Doty, and I. K Lednev, "Discrimination of human and animal blood traces via Raman spectroscopy," *Forensic Sci. Int.* **238**, 91–95 (2014).
34. M. Diem et al., "Applications of infrared and Raman microspectroscopy of cells and tissue in medical diagnostics: present status and future promises," *Spectrosc. Inter. J.* **27**, 463–496 (2012).
35. A. Benard et al., "Infrared imaging in breast cancer: automated tissue component recognition and spectral characterization of breast cancer cells as well as the tumor microenvironment," *Analyst* **139**, 1044–1056 (2014).
36. G. Cakmak et al., "FTIR spectroscopic analysis of rainbow trout liver exposed to nonylphenol," *Appl. Spectrosc.* **57**, 835–841 (2003).

37. G. Cakmak, I. Togan, and F. Severcan, "17 β-estradiol induced compositional structural and functional changes on rainbow trout liver revealed by FTIR spectroscopy: a comparative study with nonylphenol," *Aquat. Toxicol.* **77**, 53–63 (2006).
38. G. Cakmak et al., "Screening of protective effect of amifostine on radiation-induced structural and functional variations in rat liver microsomal membranes by FT-IR spectroscopy," *Anal. Chem.* **83**, 2438–2444 (2011).
39. A. Shen et al., "In vivo study on the protection of indole-3-carbinol (I3C) against the mouse acute alcoholic liver injury by micro-Raman spectroscopy," *J. Raman Spectrosc.* **40**, 550–555v (2009).
40. CytoSpec, Biomedical applications of vibrational spectroscopy—hyperspectral imaging—chemometrics, http://www.cytospec.com/ftir.php#HowToProduceMaps (2016).
41. D. Pozzi et al., "Use of EPR and FTIR to detect biological effects of ultrasound and microbubbles on a fibroblast cell line," *Eur. Biophys. J.* **40**(10), 1115–1120 (2011).
42. P. R. Griffiths and J. A. De Haseth, "*Fourier Transform Infrared Spectrometry*," John Wiley and Sons, New York (1986).
43. N.K. Afseth et al., "Raman spectra of biological samples: A study of preprocessing methods," *Appl. Spectrosc.* **60**, 1358–1367 (2006).
44. M. Severcan, P. I. Haris, and F. Severcan, "Using artificially generated spectral data to improve protein secondary structure prediction from Fourier transform infrared spectra of proteins," *Anal. Biochem.* **332**, 238–244 (2004).
45. S. Turker et al., "Investigation of compositional, structural, and dynamical changes of pentylenetetrazol-induced seizures on a rat brain by FT-IR spectroscopy," *Anal. Chem.* **86**, 1395–1403 (2014).
46. B. Elibol-Can, E. Jakubowska-Dogru, and M. Severcan, "The effects of short-term chronic ethanol intoxication and ethanol withdrawal on the molecular composition of the rat hippocampus by FT-IR spectroscopy," *Alcohol. Clin. Exp. Res.* **35**, 2050–2062 (2011).
47. K. H. Esbensen, *Multivariate Data Analysis—in Practice*, 5th ed., CAMO Process AS, Esbjerg, Denmark (2005).
48. A. Derenne et al., "FTIR spectroscopy: a new valuable tool to classify the effects of polyphenolic compounds on cancer cells," *Biochim. Biophys. Acta* **1832**, 46–56 (2013).
49. A. Sikirzhytskaya, V. Sikirzhytski, and I. K. Lednev, "Raman spectroscopy coupled with advanced statistics for differentiating menstrual and peripheral blood," *J. Biophoton.* **7**, 59–67 (2014).
50. P. Demir, S. Onde, and F. Severcan, "Phylogeny of cultivated and wild wheat species using ATR-FTIR spectroscopy," *Spectrochim. Acta A: Mol. Biomol. Spectrosc.* **135**, 757–63 (2015).
51. S. Gok et al., "Differentiation of Anatolian honey samples from different botanical origins by ATR-FTIR spectroscopy using multivariate analysis," *Food Chem.* **170**, 234–240 (2015).
52. A. Savitzky and M. J. E. Golay, "Smoothing and differentiation of data by simplified least squares procedures," *Anal. Chem.* **36**, 1627–1639 (1964).
53. F. Fassbender et al., "Simvastatin strongly reduces levels of Alzheimer's disease β-amyloid peptides Aβ42 and Aβ40 in vitro and in vivo," *Neurobiology* **98**, 5856–5861 (2001).
54. S. Youssef et al., "The HMG-CoA reductase inhibitor, atorvastatin, promotes a Th2 bias and reverses paralysis in central nervous system autoimmune disease," *Nature* **420**, 78–84 (2002).
55. L. Marcoff and P. D. Thompson, "The role of Coenzyme Q10 in statin-associated myopathy," *J. Am. Coll Cardiol.* **49**, 2231–2237 (2007).
56. K. M. Thelen et al., "Brain cholesterol synthesis in mice is affected by high dose of simvastatin but not of pravastatin," *J. Pharm. Exp. Ther.* **316**, 1146–1152 (2006).
57. F. Severcan et al., "Rapid monitoring of diabetes-induced lipid peroxidation by Fourier transform infrared spectroscopy: evidence from rat liver microsomal membranes," *Anal Biochem.* **339**, 36–40 (2005).
58. A. C. Leskovjan, A. Kretlow, and L. M. Miller, "Fourier transform infrared imaging showing reduced unsaturated lipid content in the hippocampus of a mouse model of Alzheimer's disease," *Anal. Chem.* **82**, 2711–2716 (2010).
59. N. Abdoli et al., "Mechanisms of the statins cytotoxicity in freshly isolated rat hepatocytes," *J. Biochem. Mol. Toxicol.* **27**, 287–294 (2013).
60. J. D. Vaghasiya et al., "Oxidative stress mediated hepatotoxicity Produced by simvastatin," *Pharmacologyonline* **3**, 495–503 (2008).
61. J.-C. Lin and H.-L. Liu, "Protein conformational diseases: from mechanisms to drug designs," *Curr. Drug Discov. Technol.* **3**, 145–153 (2006).
62. L. Kupfer, W. Hinrichs, and M. H. Groschup, "Prion protein misfolding," *Curr. Mol. Med.* **9**, 826–835 (2009).
63. K. Yano et al., "Katayama, Direct measurement of human lung cancerous and noncancerous tissues by Fourier transform infrared microscopy: can an infrared microscope be used as a clinical tool?," *Anal. Biochem.* **287**, 218–225 (2000).
64. D. Sheng et al., "Comparison of serum from gastric cancer patients and from healthy persons using FTIR spectroscopy," *Spectrochim. Acta Part A Mol. Biomol. Spectr.* **116**, 365–369 (2013).
65. M. L. S. Mello and B. C. Vidal, "Changes in the infrared microspectroscopic characteristics of DNA caused by cationic elements, different base richness and single-stranded form," *PLoS One* **7**, e43169 (2012).
66. H. C. Lee et al., "Increase of mitochondria and mitochondrial DNA in response to oxidative stress in human cells," *Biochem. J.* **348**, 425–432 (2000).
67. A. Mahadevan-Jansen and R. Richards-Kortum, "Raman spectroscopy for the detection of cancers and precancers," *J. Biomed. Opt.* **1**, 31–70 (1996).
68. Z. Huang et al., "Raman spectroscopy in combination with background near-infrared autofluorescence enhances the in vivo assessment of malignant tissues," *Photochem. Photobiol.* **81**, 1219–1226 (2005).
69. K. W. Short et al., "Raman spectroscopy detects biochemical changes due to proliferation in mammalian cell cultures," *Biophys. J.* **88**, 4274–4288 (2005).
70. Y. Zhou et al., "Human brain cancer studied by resonance Raman spectroscopy," *J. Biomed. Opt.* **17**, 116021 (2012).
71. M. V. Chowdary et al., "Discrimination of normal, benign, and malignant breast tissues by Raman spectroscopy," *Biopolymers* **83**, 556–569 (2006).
72. J. De Gelder et al., "Reference database of Raman spectra of biological molecules," *J. Raman Spectrosc.* **38**, 1133–1147 (2007).
73. Z. Huang et al., "Near-infrared Raman spectroscopy for optical diagnosis of lung cancer," *Int. J. Cancer* **107**, 1047–1052 (2003).
74. U. Utzinger et al., "Near-infrared Raman spectroscopy for in vivo detection of cervical precancers," *Appl. Spectrosc.* 55, 955–959 (2001).
75. G. J. Thomas and A. H. Wang. "Laser Raman spectroscopy of nucleic acids," in *Nucleic Acids and Molecular Biology*, F. Eckstein and D. M. J. Lilley, Eds., Vol. **2**, Springer-Verlag, Berlin, pp 1–30 (1988).
76. Y. Guan and G. J Thomas, "Vibrational analysis of nucleic acids. V. Force field and conformation-dependent modes of the phosphodiester backbone modeled by diethyl phosphate," *Biophys. J.* **66**, 225–235 (1994).
77. M. Ghomi et al., "Interpretation of DNA vibrational spectra by normal coordinate analysis," *Int. J. Biochem.* **22**, 691–699 (1990).

Sebnem Garip is an assistant professor in the Department of Medical Biochemistry, in Istanbul Kemerburgaz University. She received her BSc and MSc degrees in biology from Istanbul University and Middle East Technical University (METU), respectively. She received her PhD in biochemistry in METU. Her research is focused on the investigation of structural and functional effects of diseases and/or drug treatment on healthy and pathologic tissues by spectroscopic and imaging techniques for medical diagnosis and biological characterization.

Sevgi Haman Bayari received her BSc degree in physics and astronomy from Ankara University in 1981. She received her PhD in atomic and molecular physics from Gazi University in 1989. She is currently a full professor in the Physics Department at Hacettepe University. Her scientific activities have mainly focused on FTIR and Raman spectroscopy of the structural investigation of biomacromolecules.

Mete Severcan received his BSc and MSc degrees from METU and his PhD from Stanford University in 1968, 1970, and 1974, respectively. Since then he has been a member of the Department of Electrical Engineering of METU and worked as a consultant in industry. His field of interests are telecommunications, image and signal processing, application of signal processing techniques to FTIR signals for disease diagnosis, and characterization of biological systems.

Sherif Abbas is a PhD student at the Middle East Technical University. He received his MSc degree in biophysics at the Ain Shams University, Egypt, in 2007. In his MSc study, he worked on medical image analysis of white blood cells. His PhD study focuses on investigation of protein structure and dynamics using spectroscopic techniques and artificial neural networks in biomedical applications. His main research interests are molecular biophysics, spectroscopy, ANNs, and medical signal and image analysis.

Igor K. Lednev is a professor at the University at Albany, State University of New York. His research is focused on the development and application of novel laser spectroscopy for biomedical and forensic purposes. He is a fellow of the Society for Applied Spectroscopy. He served as an advisory member for the White House Subcommittee on Forensic Science. He has coauthored over 170 publications in peer-reviewed journals.

Feride Severcan received her BSc from Ankara University, Turkey, her MSc from Rochester University, USA, and her PhD from Hacettepe University, Turkey, in physics. She worked as a postdoc in the Chemistry Department of Stanford and San Francisco State Universities (USA). She has been a member of the Department of Biological Sciences at Middle East Technical University (Turkey) as a professor of biophysics since 1992. Her main interests are biological spectroscopy, medical diagnostics, drug-biological system interactions, and ecotoxicology.